Structural Nonlinearity Identification and Steady-State Behavior Prediction from Transient Aeroelastic Data

Y.S. Wong
Department of Mathematical and Statistical Sciences,
University of Alberta, 632 C.A.B.,
Edmonton, Alberta, T6G 2G1, Canada
yaushu.wong@ualberta.ca

C. A. Popescu
Department of Mathematical and Statistical Sciences,
Grant MacEwan College, 10700-104 Ave,
Edmonton, Alberta, T5J 4S2, Canada

B.H.K. Lee
BHK Lee Consulting,
Ottawa, Ontario, K1V 9B1, Canada

ABSTRACT

This paper presents a data-driven approach to predict the steady-state response utilizing information from the transient data. The aeroelastic system investigated is a two degree-of-freedom airfoil oscillating in pitch and plunge. First the method identifies the specific type of the structural nonlinearity. Appropriate state-space formulations are then proposed to model aeroelastic systems with continuous or piece-wise linear structural nonlinearity. The Kalman filter and the expectation maximization algorithm are employed to estimate the system parameters, and the steady-state behavior is then predicted from the reconstructed state-space model. Results using experimental data and numerically simulated data for an aeroelastic system with freeplay and polynomial spring are reported to demonstrate the performance of the proposed method.

NOMENCLATURE

α	pitch angle
ξ	non-dimensional plunge displacement
M_0	preload
δ	freeplay

α_f	beginning of the freeplay
x_α	non-dimensional distance from elastic axis to centre of mass
U^*	non-dimensional velocity
ζ_α, ζ_ξ	viscous damping ratios in pitch and plunge
r_α	radius of gyration about elastic axis
μ	airfoil/ air mass ratio
$\|\cdot\|$	the absolute value of a complex number
t	non-dimensional time
$K(\cdot)$	Kernel function
$E[\cdot]$	expected value
$E[\cdot\|\cdot]$	conditional expectation
N	number of observations
h_N	bandwidth parameter

Superscript

$'$	first order time derivative
$''$	second order time derivative
^{t}	transpose of a vector or matrix

1 INTRODUCTION

Prediction of aeroelastic behavior has been a subject of research for many years. For obvious reasons related to flight safety, it is important to develop methods which are capable of forecasting the steady-state behavior of aircraft structures or control surfaces. Knowing the possibility of encountering divergent flutter, limit-cycle oscillations, or chaotic behavior before they occur can help to prevent catastrophic consequences due to structural failure.

In this paper, we consider a two-degree-of-freedom (DOF) aeroelastic system which simulates an oscillating airfoil in pitch and plunge. In general, nonlinearity arises either from the aerodynamics or from the structure. If the flow is in the low speed regime, linear aerodynamics can be assumed. Thus, the only source of nonlinearity is due to the structure which may occur in the restoring forces and can be classified as a continuous type, for example, polynomial springs, or piece-wise linear type such as freeplay and hysteresis. The distinct characteristics of the freeplay or hysteresis is the existence of the switching points. Even though a system of nonlinear differential equations is generally used to model a nonlinear aeroelastic system, the mathematical formulation can be rewritten as a set of linear systems for aeroelastic models with piece-wise linear structures.

Traditional methods in the study of nonlinear aeroelasticity include experimental investigations, numerical simulations and various mathematical techniques ([4],[5],[10],[12]). In recent years, there has been a growing interest in developing data-driven procedures from aeroelastic data. In our earlier study ([25],[24],[16]),

we proposed an expert data mining system for aeroelastic predictions. Using limited transient data as input, artificial neural networks and nonlinear time series models were developed to predict the asymptotic state of the aeroelastic systems. Even though these techniques have been tested on the simulated data and experimental data, it is not easy to justify the success in using neural networks, and it is also a difficult task in searching a suitable nonlinear model to fit aeroelastic data in using a time series approach. To develop a reliable data-driven predictor in aeroelasticity applications, we present another approach in this paper. The proposed method utilizes a system identification technique which has been applied to solve a wide range of engineering problems. The important feature of the present approach is that the specific type of the structural nonlinearity is first identified from the transient data. Appropriate mathematical formulations are then constructed to model aeroelastic systems with continuous or piece-wise linear structures. Once a model is chosen, the associated system parameters are estimated by iterative parameter estimation procedures such as the Kalman filtering and the expectation - maximization algorithm [17]. Consequently, we can forecast the steady-state response from the reconstructed aeroelastic model.

2 AEROELASTIC MODEL

Consider a two degree-of-freedom (DOF) aeroelastic system which simulates an oscillating airfoil in pitch and plunge. Mathematically, the model with subsonic aerodynamics can be described by the following system of equations:

$$\xi'' + x_\alpha \alpha'' + 2\zeta_\xi \frac{\tilde{\omega}}{U^*}\xi' + \left(\frac{\tilde{\omega}}{U^*}\right)^2 G(\xi) = -\frac{1}{\pi\mu}C_L(t) \tag{1}$$

$$\frac{x_\alpha}{r_\alpha^2}\xi'' + \alpha'' + 2\frac{\zeta_\alpha}{U^*}\alpha' + \frac{1}{U^{*2}}M(\alpha) = \frac{2}{\pi\mu r_\alpha^2}C_M(t), \tag{2}$$

where x_α, r_α, ζ_α, ζ_ξ, $\tilde{\omega}$, U^*, μ are the airfoil parameters, and they are defined in Ref. [10]. Here $G(\xi)$ and $M(\alpha)$ are the nonlinear plunge and pitch stiffness terms, respectively. $C_L(t)$, $C_M(t)$ are the lift and pitching moment coefficients. For an incompressible flow, $C_L(t)$ and $C_M(t)$ can be expressed by the integral terms as shown in Ref. [10].

In the current study, we consider the structural nonlinearity is imposed only in the pitch DOF, and it can be taken as one of the following types.

Polynomial spring:

$$M(x) = a_n x^n + \ldots + a_1 x + a_0. \tag{3}$$

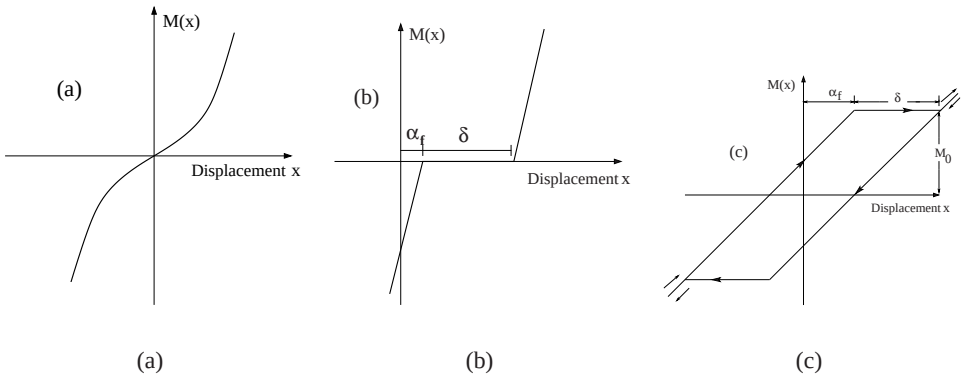

Figure 1: General sketches for the structural nonlinearities (a) polynomial spring (b) freeplay (c) hysteresis

Freeplay:

$$M(x) = \begin{cases} x - \alpha_f & \text{if } x < \alpha_f \\ 0 & \text{if } \alpha_f \leq x \leq \alpha_f + \delta \\ x - \alpha_f - \delta & \text{if } x > \alpha_f + \delta. \end{cases} \tag{4}$$

Hysteresis:

$$M(x) = \begin{cases} x - \alpha_f + M_0 & \text{if } x < \alpha_f \uparrow \\ x + \alpha_f - M_0 & \text{if } x > -\alpha_f \downarrow \\ M_0 & \text{if } \alpha_f \leq x \leq \alpha_f + \delta \uparrow \\ -M_0 & \text{if } -\alpha_f - \delta \leq x \leq -\alpha_f \downarrow \\ x - \alpha_f - \delta + M_0 & \text{if } x > \alpha_f + \delta \uparrow \\ x + \alpha_f + \delta - M_0 & \text{if } x < -\alpha_f - \delta \downarrow . \end{cases} \tag{5}$$

Here, $\uparrow$ and $\downarrow$ denote the motion in increasing or decreasing $x-$ direction. The general sketches for the structural nonlinearities are shown in Fig. 1.

By introducing four new variables ω_1, ω_2, ω_3, ω_4, the integro-differential system (1) - (2) can be rewritten as an 8-DOF system of ordinary differential equations:

$$\mathbf{X}_t^{'} = \mathbf{A}\mathbf{X}_t + F(\mathbf{X}_t), \tag{6}$$

where $\mathbf{A}$ is a matrix containing the system coefficients, F is a non-linear function, and $\mathbf{X} = [\alpha, \alpha^{'}, \xi, \xi^{'}, \omega_1, \omega_2, \omega_3, \omega_4]^t$. The complete system can be found in Ref. [10]. The coefficients in F are zero except for the second row which is due to the non-zero coefficients $a_k x^k$ for $k > 1$ in the polynomial spring in the pitch DOF. For a structural nonlinearity represented by a piece-wise linear type,

the aeroelastic model can be expressed by a set of linear systems. For example, for a freeplay model, there exists two switching points. If the freeplay parameters α_f and δ are known, the corresponding aeroelastic model can be divided into three regions in which each region is governed by a linear system. The corresponding aeroelastic model can be written as

$$\begin{cases} X_t' &= AX_t + F_1 \text{ if } X_t(1) < \alpha_f, \\ X_t' &= BX_t + F_2 \text{ if } \alpha_f \leq X_t(1) \leq \alpha_f + \delta, \\ X_t' &= AX_t + F_3 \text{ if } X_t(1) > \alpha_f + \delta, \end{cases} \tag{7}$$

where $X(1) = \alpha$ is the first component of the 8-DOF vector X. Here, A and B are 8×8 matrices, and F_i, $i = 1, 2, 3$ are eight-dimensional vectors. Although the paper is focused on the structural nonlinearity represented by polynomial spring and freeplay, the techniques discussed here can be extended directly to the hysteresis case.

In the present aeroelastic model, the two physical variables are given by the pitch angle and plunge displacement. Suppose limited aeroelastic transient data are known, the goal of this paper is to describe a data-driven tool utilizing the system identification technique to forecast the steady-state response of the aeroelastic system. In general, identification techniques for linear time invariant systems are well developed. Efficient software such as the MATLAB system identification tool box is available for problems in engineering applications. However, non-linear system identification techniques are less advanced than those for the linear systems, and selecting an appropriate mathematical model that provides a true representation of the physical system is often a difficult task.

In developing a data-driven method, we start with a time series of measured data. In Fig. 2, samples of transient aeroelastic data are displayed. Due to the space constraint, only one of the time-histories of either the pitch angle or the plunge displacement is shown. However, in actual applications, both the pitch and plunge data are employed. The time series illustrated in Fig. 2 have not reached the steady-state, and they are generated by experiments or numerical simulations. Fig. 2a is from experiment for an aeroelastic model with a polynomial spring, 2b and 2c are from experiments with a freeplay, and 2d is from numerical simulation for a freeplay. Obviously, it is difficult to forecast the steady-state response based on the limited data. In each case, the long-term behavior could be a limit-cycle-oscillation, non-oscillating fixed-point solution, divergent, or even a chaotic motion.

In Section 3, we first describe statistical techniques which are capable of identifying the specific type of the structural nonlinearity from the limited data. Knowing that the data is arising from aeroelastic systems with continuous or piece-wise linear structures enables us to construct an appropriate mathematical model which exhibits a nonlinear response consistent with the known transient data. The un-

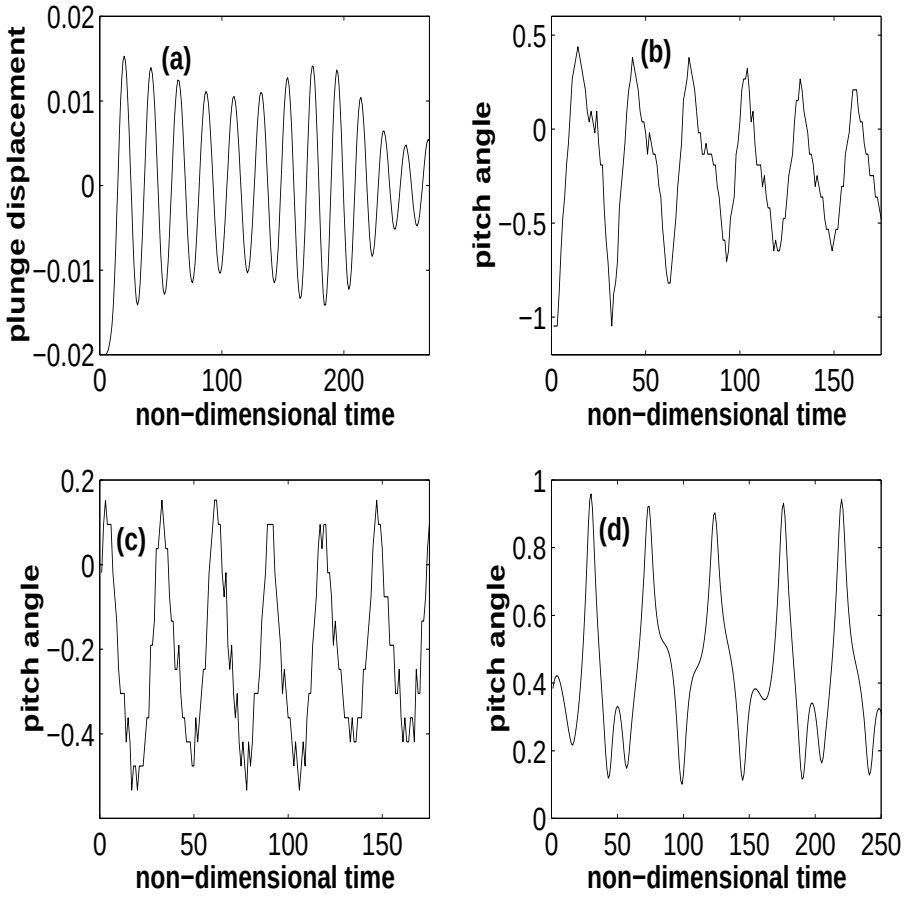

Figure 2: Samples of input pitch data for data-driven method

known parameters in the developed model are estimated by the Kalman filter and the expectation maximization algorithm, and this is reported in Section 4. Finally, Section 5 presents several case studies which serve to validate the capability of the proposed data-driven method.

3 STRUCTURAL NONLINEARITY IDENTIFICATION

Spectral analysis has been used to detect nonlinearity in a wide range of problems in science and engineering. For example, estimated bispectral have been used to study non-linear transfer of energy in turbulence [11, 23], in plasma physics[9], and investigation of quadratic coupling between the frequencies associated with the dynamics of a nonlinear mechanical system [7]. Higher order spectral methods have been applied to simulated aeroelastic data with polynomial structural

non-linearities [21], wind-tunnel data [6], and flight test data [20]. Moreover, the trispectrum [3] was employed to identify the aeroelastic cubic non-linearities.

Consider $\{X(n)\}, n = 1 \ldots, N$, as a stationary time series with mean $E[X(n)] = 0$, otherwise we work with the mean deleted series. The bispectrum of $\{X(n)\}$ is a two-dimensional Fourier transform of the third-moment function $C(n, m) = E[X(k + n)X(k + m)X(k))]$:

$$B(\omega_1, \omega_2) = \sum_m \sum_n C(n, m) exp\{-2\pi i\omega_1 n - 2\pi i\omega_2 m\}. \tag{8}$$

The bicoherence is the normalized bispectrum:

$$b(\omega_1, \omega_2) = \frac{|B(\omega_1, \omega_2)|}{\sqrt{B(\omega_1)B(\omega_2)B(\omega_1 + \omega_2)}}. \tag{9}$$

Since the bispectrum is a spatially periodic function, its values in the plane are completely determined by the values in the principal domain $\{(\omega_1, \omega_2) : 0 < \omega_1 < 0.5, \omega_2 < \omega_1, 2\omega_1 + \omega_2 < 1\}$. A detailed theoretical study of higher order spectra is presented in Ref. [2].

It has been well recognized that the bispectrum and the bicoherence of a Gaussian signal are identically zero, and a large magnitude of the bispectrum indicates a quadratic coupling or a nonlinear interaction among different frequency components of a signal. Hence, by inspecting the bispectrum plots resulting from aeroelastic data, we can confirm the structural nonlinearity from the presence of large spectral amplitudes shown in the bispectrum plots. However, the bispectrum and bicoherence can not distinguish whether the nonlinearity is of the continuous or piece-wise linear type. To identify a specific structural nonlinearity such as polynomial spring, freeplay or hysteresis, we consider a non-parametric statistical method.

The self-exciting threshold auto-regressive (SETAR) is a nonlinear statistical model which was first proposed by Tong [22]. The SETAR is a piece-wise linear process in which a time series is divided into j regimes according to j-1 thresholds. In each regime, a different auto-regressive model is applied. Let $\{t_0, t_1, \ldots, t_l\}$ denote the thresholds, i.e., a linearly ordered subset of real numbers, such that $t_0 < t_1 < \ldots < t_l$, where $t_0 = -\infty$ and $t_l = +\infty$. A self-exciting threshold autoregressive model of order $(l; p, \ldots, p)$ or SETAR $(l; p, \ldots, p)$ where p is repeated l times, is a uni-variate time series $\{X_n\}$ of the form

$$X_n = a_0^{(j)} + \sum_{i=1}^{p} a_i^{(j)} X_{n-i} + e_n, \quad t_{j-1} < X_{n-d} \leq t_j, \tag{10}$$

for $j = 1, 2, \ldots l$, where d is a fixed integer belonging to $\{ 1, 2, \ldots, p\}$, and $\{e_n\}$ is a Gaussian, independent, identically distributed white noise sequence. If for

$j = 1, 2, \ldots, l$, we have $a_i^{(j)} = 0$ for $i = p_j + 1, p_j + 2, \ldots, p$, then $\{X_n\}$ is known as a SETAR$(l; p_1, p_2, \ldots, p_l)$ model. Hence, a SETAR $(1, p)$ model is equivalent to a linear autoregressive (AR) model of order p.

Let us define the vector $\mathbf{Y}_n = (X_n, \ldots, X_{n-p+1})^t$, then a SETAR$(l; p, p, \ldots, p)$ model can be rewritten in a discrete state-space form:

$$\mathbf{Y}_n = f(\mathbf{Y}_{n-1}) + \mathbf{E}_n, \tag{11}$$

where $\mathbf{E}_n = (e_n, 0, \ldots, 0)^t$, $f(\mathbf{Y}_{n-1}) = (h(\mathbf{Y}_{n-1}), X_{n-1}, \ldots, X_{n-p+1})^t$, and $h(\mathbf{Y}_{n-1})$ is given in the right side of the Eq. (10).

The key task in the SETAR models is to determine the thresholds and the delay parameter d, and this can be achieved by carrying out a non-parametric lag regression estimation $m_j(x) = E[X_n | \, X_{n+j}]$. Let h_N denote the bandwidth parameter, and let $K(\cdot)$ be a kernel function which is usually a continuous probability density function: $K(u) \geq 0$ and $\int K(u)du = 1$. A non-parametric kernel estimate $\hat{m}_j(x)$ for $m_j(x)$ can be expressed by

$$\hat{m}_j(x) = \sum_{i=-j+1}^{N} X_i K_N(x - X_{i+j}) / \sum_{i=-j+1}^{N} K_N(x - X_{i+j}), \tag{12}$$

for $j = -s, \ldots, -1$, where s is a positive integer much smaller than the size N of the data set. A simple kernel function is given by the triangular kernel [22] where

$$K_N(u) = \begin{cases} (1 - |u|/h_N)/h_N & \text{if } |u| \leq h_N \\ 0 & \text{otherwise.} \end{cases} \tag{13}$$

The choice of the kernel is not critical in practical implementations, and other types such as the Epanechnikov kernel or the Gaussian kernel can also be employed. It is worth mentioning that similar formula can be developed for the non-parametric estimates $\hat{v}_j(x)$ of the variance $v_j(x) = VAR(X_n | \, X_{n+j})$. Hence, by analyzing the plots of $\hat{m}_j(x)$ and $\hat{v}_j(x)$ for various values of j, the values of the thresholds and the delay parameter can be estimated.

Now, recall that for an aeroelastic system with a piece-wise linear structure such as freeplay, the aeroelastic model can be expressed as a system of linear equations given in Eq. (7). Using a sufficiently small sampling step τ, the following state-space formulation is resulted:

$$\begin{aligned} X_{t+\tau} &= A_1(\tau)X_t + b_1(\tau) \text{ if } X_t(1) < \alpha_f, \\ X_{t+\tau} &= A_2(\tau)X_t + b_2(\tau) \text{ if } \alpha_f \leq X_t(1) \leq \alpha_f + \delta, \\ X_{t+\tau} &= A_3(\tau)X_t + b_3(\tau) \text{ if } X_t(1) > \alpha_f. \end{aligned} \tag{14}$$

Here, A_i, $i = 1, 2, 3$ are 8×8 matrices, $A_3 = A_1$, and b_i, $i = 1, 2, 3$ are eight-dimensional vectors. It is then clear that there are many common features among

the state-space formulations arising from the SETAR model and the freeplay model. In particularly, both models exhibit the piece-wise linear characteristic, in which the changes depend on the values of the thresholds and delay parameters in SETAR and on the switching points in freeplay. Hence, to distinguish the structural nonlinearities associated with a continuous type such as polynomial spring, or piece-wise linear cases such as freeplay or hysteresis from given aeroelastic data, we can apply a non-parametric estimation. By confirming the existence of the switching points, we can identify the specific type of the structural nonlinearity.

4 ESTIMATION OF SYSTEM PARAMETERS

Once a mathematical model is determined, the remaining task is to estimate the associated system parameters using the information from the known measured data. For example, for a freeplay model given in Eq. (14), if the matrix coefficients A_i and the vector b_i are known, the nonlinear behavior of the aeroelastic system can be predicted from the reconstructed freeplay model.

Let us consider the state-space form of a general nonlinear discrete system

$$\begin{aligned} x_{k+1} &= f[x_k, u_{k+1}] + v_{k+1}, \\ y_{k+1} &= h[x_{k+1}, u_{k+1}] + w_{k+1}. \end{aligned} \tag{15}$$

Here $f[\cdot,\cdot]$ is the process model, x_k is the state of the system at the k-time step, u_k is the input vector, y_k is the observation vector, $h[\cdot,\cdot]$ is the observation model, v_k is the noise process and w_k is the additive measurement noise. We assume that the noise vectors, v_k and w_k, are Gaussian and from uncorrelated white sequences: $E[v_k] = E[w_k] = 0$, for all k, and $E[v_i v_j^t] = \delta_{ij} Q_i$, $E[w_i w_j^t] = \delta_{ij} R_i$, $E[v_i w_j^t] = 0$, for all i, j, where δ_{ij} is the Kronecker symbol. We use the notations $\bar{x}_i = E[x_i | y_1, \ldots, y_i]$ and $\hat{x}_{i+1} = E[x_{i+1} | y_1, y_2, \ldots, y_i]$ for the filtered and the predicted values, respectively. The corresponding conditional covariances are $\bar{P}_i = E\left[(x_i - \bar{x}_i)(x_i - \bar{x}_i)^t | y_1, \ldots, y_i\right]$ and $\hat{P}_{i+1} = E\left[(x_{i+1} - \hat{x}_{i+1})(x_{i+1} - \hat{x}_{i+1})^t \mid y_1, \ldots, y_i\right]$. The classical Kalman update equations ([1], Chapter 4) at time $k+1$ are given by

$$\begin{aligned} \bar{x}_{k+1} &= \hat{x}_{k+1} + G_{k+1} \nu_{k+1}, \\ \bar{P}_{k+1} &= \hat{P}_{k+1} - G_{k+1} \hat{P}_{\nu_{k+1}\nu_{k+1}} G_{k+1}^t. \end{aligned}$$

Here, $\nu_{k+1} = y_{k+1} - \hat{y}_{k+1}$ is the innovation, $\hat{P}_{\nu_{k+1}\nu_{k+1}}$ is the conditional covariance and $G_{k+1} = \hat{P}_{x_{k+1}y_{k+1}} \hat{P}^{-1}_{\nu_{k+1}\nu_{k+1}}$ is the Kalman gain. To calculate these quantities both the extended Kalman filter (EKF) and the unscented filter (UF) [8] approximate the state distribution with a Gaussian one. However, instead of using the EKF linearization approach, the UF employs a deterministic sampling.

The sample points completely capture the true mean and the true covariance. In contrast to the first-order accuracy of the EKF, the UF is capable of accurately capturing the true posterior mean and the covariance up to the third order for a nonlinear system. Moreover, the UF is computationally more attractive, it does not require the calculations of the Jacobians, and it can apply to aeroelastic systems with structural nonlinearities given by freeplay and hysteresis models.

The expectation maximization (EM) algorithm [14] is a popular engineering tool for estimation of parameters [19]. The EM algorithm is particularly useful when it is straightforward to compute the likelihood of the model using not only the observed data Y_{obs}, but also the hidden data Y_{hid}. In the present study, although the measured data are given by the pitch angle and the plunging displacement, the aeroelastic model include their derivatives. The derivatives are regarded as the hidden data. The EM algorithm is implemented by a data augmentation scheme, such that the observed data are a mapping of the augmented data $Y_{obs} = M(Y_{aug})$, where $Y_{aug} = \{Y_{obs}, Y_{hid}\}$. The algorithm starts with an initial guess θ_0 for the unknown parameters and iteratively improve the estimation θ^*. At each iteration, the EM algorithm consists of two steps: the expectation (E) step which computes the expectation of the likelihood; and the maximization (M) step which computes the updated estimations of the parameters by maximizing the results obtained in the E step.

More precisely, using the current estimation θ_n of the parameters, the E-step computes the conditional expectation of the augmented data log-likelihood $Q(\theta|\theta_n)$ = $E[\log p(\theta|Y_{aug})|\, Y_{obs}, \theta_n]$. An approximation may be required during the E-step. In order to justify the convergence, it is important to note that the negative of the free-energy is maximized [14] with respect to the distribution component:

$$Q_{n+1} = \arg\max_{Q} \mathcal{F}(Q, \theta_n), \tag{16}$$

where

$$\mathcal{F}(Q, \theta) = \int Q(Y_{hid}) \log p(\theta|Y_{aug}) \mathrm{d}Y_{hid} - \int Q(Y_{hid}) \log Q(Y_{hid}) \mathrm{d}Y_{hid}. \tag{17}$$

The M-step performs maximization with respect to the parameters θ:

$$\theta_{n+1} = \arg\max_{\theta} Q(\theta|\theta_n). \tag{18}$$

In term of $\mathcal{F}$, the M-step can be expressed as:

$$\theta_{n+1} = \arg\max_{\theta} \mathfrak{F}(Q_{n+1}, \theta). \tag{19}$$

Hence, an approximation can be used either in the E-step or the M-step as long as $\mathcal{F}$ is increasing.

An important feature of the EM-algorithm for parameter estimation is the guaranteed of convergence ([26]), [14]). However, depending on the initial guess, the algorithm may only converge to a local maximum.

Using the filtered values $\bar{x}_i$ and $\bar{P}_i$, in the E step we calculate the smoothed values $x_i^N = E[x_i|y_1,\ldots,y_N]$, $P_i^N = E[(x_i - x_i^N)(x_i - x_i^N)^t|y_1,\ldots,y_N]$, and $P_{i,i-1}^N = E[(x_i - x_i^N)(x_{i-1} - x_i^N)^t|y_1,\ldots,y_N]$. In the M step, the smoothed values are replaced in the formulas for updating the estimations of the parameters.

We now briefly describe the implementation of the EM algorithm for the aeroelastic system given in Eqs. (1)-(2). For a freeplay model, the mathematical formulation can be expressed by the set of linear systems given in Eq. (14). Since only α and ξ are observed in practice, Eq. (14) can be rewritten as a linear discrete switching state-space system:

$$\begin{cases} x_{k+1} &= A_{S_{k+1}} x_k + b_{S_{k+1}} + v_{k+1}, \\ y_k &= Cx_k + w_k, \end{cases} \tag{20}$$

where S_{k+1} is a discrete random variable given by

$$S_{k+1} = \begin{cases} 1 & \text{if } x_k(1) < \alpha_f, \\ 2 & \text{if } \alpha_f \leq x_k(1) \leq \alpha_f + \delta, \\ 3 & \text{if } x_k(1) > \alpha_f + \delta, \end{cases} \tag{21}$$

where, A_i and b_i, $i = 1,2,3$ are defined in Eq. (14), $y_k = [\alpha, \xi]^t$ is the two-dimensional observation vector, $x_k = [\alpha, \alpha^{'}, \xi, \xi^{'}, \omega_1, \omega_2, \omega_3, \omega_4]_k^t$ is the eight-dimensional state vector, $v_k \sim N(0, Q_{S_k})$ and $w_k \sim N(0, R)$ are independent Gaussian white noise vectors, Q_i, $i = 1,2,3$ are 8×8 matrices, R is a 2×2 matrix, and C is the 2×8 matrix

$$C = \begin{bmatrix} 1 & 0 & 0 & \ldots & 0 \\ 0 & 1 & 0 & \ldots & 0 \end{bmatrix}. \tag{22}$$

Once α_f and δ are estimated using the non-parametric method presented in the previous section, the values of the switching variable S_k are known. Moreover, we assume that when $S_1 = i$, we have $x_1 \sim N(\mu_i, \Sigma_i)$, for $i = 1,2,3$. Hence, the unknown parameters of the previous model are $\Theta = \{A_i, b_i, Q_i, R, \mu_i, \Sigma_i, i = 1,2,3\}$. The linear Kalman filter can be used to calculate the smoothed values x_i^n, P_i^n and $P_{i,i-1}^n$. The details of the implementation of the EM algorithm, the log-likelihood and the updating formulas are reported in [15].

It is worth noting that the complexity of the parameter estimation process depends on the number of unknown parameters Θ. For a matrix of order eight, there are 64 unknown coefficients to be estimated. However, in $\mathbf{X} = [\alpha, \alpha^{'}, \xi, \xi^{'}, \omega_1, \omega_2, \omega_3, \omega_4]^t$, only the first four are physical variables, and the remaining four are introduced to eliminate the integral formulations from the aerodynamic terms. Hence,

for a two DOF aeroelastic system, it is reasonable to consider a reduced model with $\mathbf{X} = [\alpha, \alpha^{'}, \xi, \xi^{'}]^t$. Using this model, the number of the unknown parameters is greatly reduced. For a matrix of order four, 16 unknown coefficients need to be determined. From the results to be presented in the case studies in section 5, it is clear that the reduced system is as effective as the full model in predicting the aeroelastic behavior.

Next, we present the EM algorithm for an aeroelastic system with a polynomial restoring force given in pitch, where

$$M(x) = a_5x^5 + a_4x^4 + a_3x^3 + a_2x^2 + a_1x + a_0. \tag{23}$$

Consider a reduced system consisting of the pitch angle, plunge displacement and their derivatives, and using a simple Euler integration scheme, the associated reduced discrete system can be expressed as:

$$x_{k+1} = Ax_k + \begin{bmatrix} 0_{2\times4} \\ B \end{bmatrix} [x_k^2(1), x_k^3(1), x_k^4(1), x_k^5(1)]^t + \begin{bmatrix} 0_{2\times1} \\ b \end{bmatrix} + v_{k+1},$$
$$y_{k+1} = \begin{bmatrix} 1 & 0 & 0 & 0 \\ 0 & 1 & 0 & 0 \end{bmatrix} x_{k+1} + w_{k+1}.$$

Here $x_k = [\alpha, \xi, \alpha^{'}, \xi^{'}]^t$ is the state of the system at time step k, and $y_{k+1} = [\alpha, \xi]^t$ is the observation vector. We assume that the white noise vectors, v_k and w_k, are Gaussian and from uncorrelated white sequences. The 4×4 matrix A, the 2×4 matrix B, the two dimensional vector b , and the two covariance Q and R matrices corresponding to the noise vectors v_k and w_k represent the unknown parameters Θ of the aeroelastic system. Once the parameters are estimated, we can predict the future values of x_i, $i = N + 1, N + 2, \ldots$, and consequently the steady-state behavior of the aeroelastic model.

In estimating the parameters Θ using the EM algorithm, we first augment the data with the hidden variables x_i, $i = 1, \ldots, N$ and then calculate the complete log-likelihood:

$$\log(L) = \log P(x_1, \ldots, x_N, y_1, \ldots, y_N) = \log P(y_N|y_{N-1}, \ldots, y_1, x_N, \ldots, x_1)$$
$$+ \ldots + \log P(y_1|x_N, \ldots, x_1) + \log P(x_N|x_{N-1}, \ldots, x_1) + \ldots + \log P(x_1).$$

Unlike the freeplay model, the present system has a nonlinear state equation. In the E-step, the likelihood and the conditional expectation of the likelihood $\hat{E} = E[\log(L)|y_1, \ldots, y_N]$ is approximated based on the linearization of the previous system. The formulas are similar to those reported [19] in the linear case, but we have to employ EKF or the UF to compute the conditional expectations x_n^N, variances P_n^N, and covariances $P_{n,n-1}^N$. In the M-step, analytical update equations for the parameters Θ can be found by taking the derivatives with respect to the parameters Θ in the formula for $\hat{E}$ [19].

5 RESULTS AND DISCUSSIONS

In order to evaluate the effectiveness of the techniques presented in the previous sections, we consider the following case studies in this section.

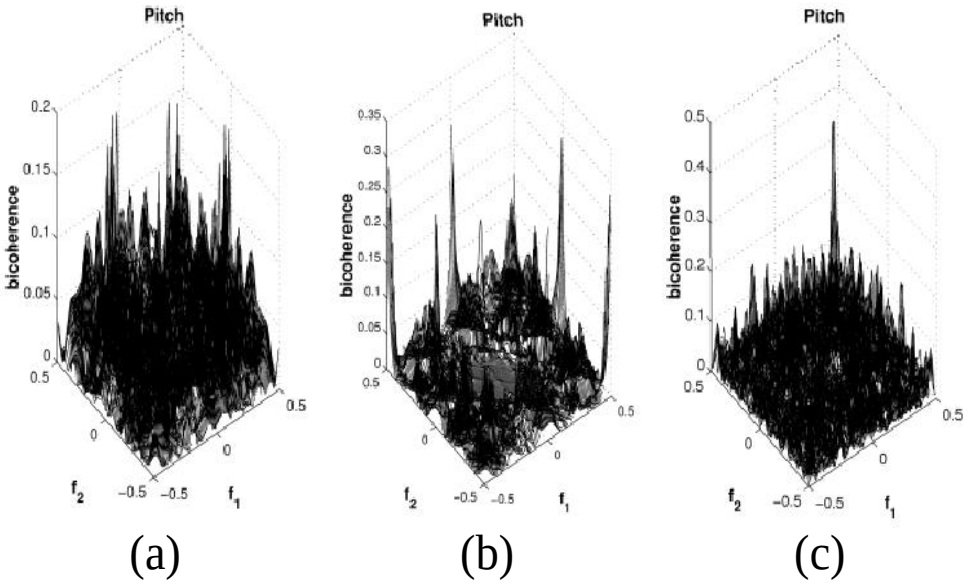

Figure 3: Bicoherence plots for aeroelastic data (a) polynomial spring (b) freeplay (c) hysteresis

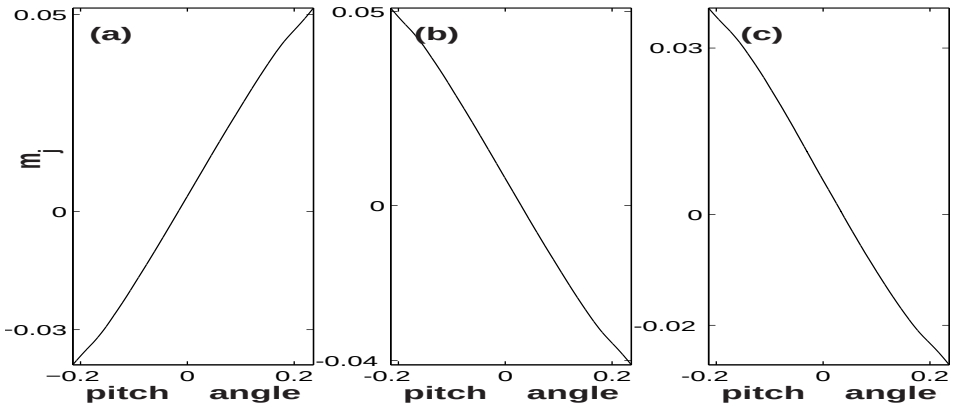

Figure 4: Estimated mean for aeroeelastic data with polynomial spring (a) $j = -1$ (b)$j = -10$ (c) $j = -30$

In Fig. 3, we present the bicoherence plots for three data sets 'a', 'b' and 'c' representing the pitch motions. The data are similar to those displayed in Fig.2,

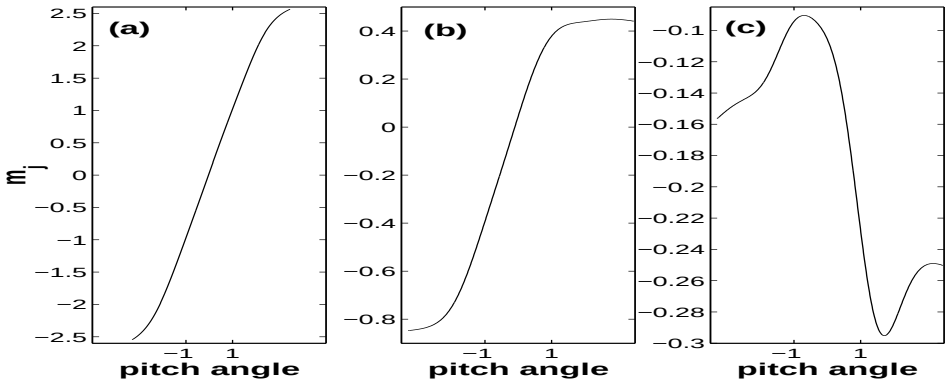

Figure 5: Estimated means for experimental freeplay data: (a) $j = -4$ (b) $j = -10$ (c) $j = -12$

in which two sets 'a' and 'b' are resulted from experiments corresponding to an aeroelastic model with polynomial spring and freeplay in pitch, and the remaining set 'c' is generated numerically from solving Eqs. (1)-(2) with a structural nonlinearity represented by a hysteresis in the pitch DOF. Notice that the bicoherence plots share a common feature namely several large spectral peaks are observed. Similar bicoherence plots are noted by using the corresponding data in the plunge DOF. Hence, it is easy to conclude that these data exhibit nonlinearity. However, we definitely can not identify which data set corresponds to an aeroelastic model with polynomial spring, freeplay or hysteresis based on the information solely from these plots.

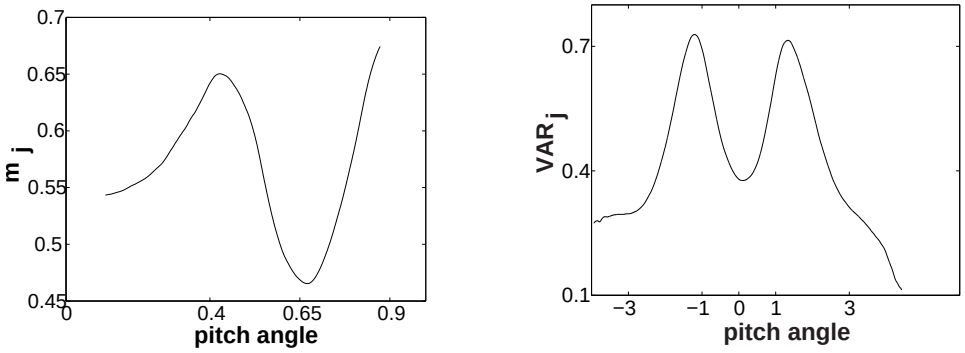

(a) (b)

Figure 6: Non-parametric estimates (a) mean $j = -18$ (b) variance $j = -1$

Now, we demonstrate that by applying a nonparametric study with the same data, we can identify the specific type of structural nonlinearity with confidence.

In Figs. 4 - 6, we display the nonparametric estimates of the mean or the variance from the given aeroelastic data. The plots shown in Fig. 4 indicate that the estimated means for various values of j are well approximated by straight lines. This in turns reveals that the data is associated with a continuous nonlinearity, such as a polynomial spring in our case. Recall that the most distinct characteristics in performing a nonparametric study is to identify the existence of the switching points.

Fig. 5 illustrates the behavior of the estimated mean of a typical freeplay data as the value of j increases. Initially when $j = -4$, the plot resembles a straight line as those shown in Fig. 4 from a polynomial spring data. However, when $j = -10$, it will not be well approximated by a straight line, and when $j = -12$, the maximum and minimum points are clearly visible. The extreme values confirm the existence of the switching points. Since only two switching points are identified, we conclude that the data is associate with a freeplay model. From the locations of the extreme values, we could also estimate the freeplay parameters α_f and δ. In Fig. 6 (a), we show the estimated mean for another freeply data set with $\alpha_f = 0.4$ and $\delta = 0.25$. The plot clearly shows the presence of two switching points. Fig. 6(b) reveals that the plot of the estimated variance contains three extreme values, hence it can not represent a freeplay. In general, we expect four switching points in a hysteresis as shown in Fig. 1. However, when α_f is zero, the two switch points coincide at the same location. Hence, there are only three distinct locations for the switching points. Here, the extreme values are located at -1, 0, and +1. The data correspond in Fig.6(b) is indeed from an aeroelastic system with hysteresis. The nonparametric estimation have been tested on many aeroelastic data, and it is a reliable and robust procedure to distinguish the specific type of structural nonlinearity associated with an aeroelastic model. It is also worth mentioning that when carrying out a nonparametric study, accurate conclusions can be reached using a very limited transient data (typically less than 300 data points).

In Fig. 7, we show the convergence of the EM algorithm for estimation of system parameters. From the plot of the log-likelihood versus the number of EM cycles, we observe that after a rapid convergence at the beginning, the convergent rate is then improving very slowly. This is a typical characteristics of the EM algorithm [13] for all cases being investigated in this work. In practical implementations, the EM algorithm is usually terminated when the improvement becomes small. For the particular case shown in Fig. 7, it is sufficed to stop the EM algorithm after thirty cycles.

In Fig. 8, results of steady state predictions using aeroelastic data are presented. In each case, about 200 data points (as indicated by the two vertical lines in the figure) are used to carry out the nonparametric study and parameter estimations. To validate the proposed model and the reconstructed system, a small number of data about 40 points are taken after the training set to compare the predicted value

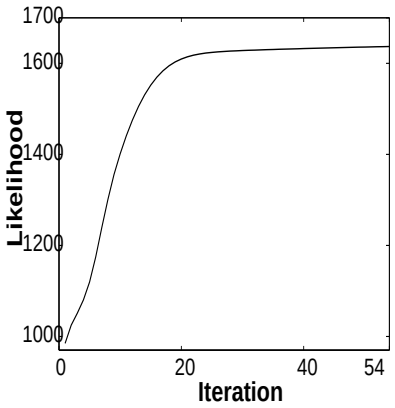

Figure 7: Convergence of the EM algorithm

and the known data. The discrepancy between these values provides a degree of the confidence in the prediction for a long-term behavior. Large errors clearly indicate the failure of the method. In the figures, the prediction is represented by a dash line and the original pitch motion is given in a solid line. The results for the corresponding plunge DOF are similar, and will be omitted. The time series presented in Figs. 8a - 8c correspond to experimental data in which (a) and (b) are from a freeplay model, and (c) is associated with a polynomial spring. The experiment investigations were conducted at the McGill University and the Texas A&M University. The results demonstrate the overall performance of the proposed data-driven technique. The time history displayed in Fig. 8a and 8b correspond to the same case, the amplitude of the pitch motion decreases initially, and then follows by a period with almost a constant amplitude before reaching a fixed-point value. Although the correct fixed-point response is forecasted in Fig. 8a, it occurs early than the experiment data. Using a section of the data taken in the region with almost a constant amplitude, excellent agreement is achieved as shown in Fig 8b.

We have carried out many test cases in which the steady-state behaviors include limit-cycle-oscillation, fixed-point solution and divergent motion, and the predicted responses are in good agreement with the original data [15]. Finally, to investigate the limit of the developed data-driven tool, we consider a chaotic motion as shown in Fig. 9. The time history is generated from a freeplay model and was previously studied by Price, Alighambari and Lee [18]. In Fig. 10, we present the evolution of the phase space. The chaotic motion is identified by the "two-well potential" phase-trajectory in the α - $\alpha^{'}$ plane displayed in Fig. 10d. However, if we only consider the first 600 data, the phase plot reveals only one-well potential structure as shown in Fig. 10a. From the time history shown in Fig. 9, we notice a change in the profile occurs around $t = 600 - 700$. Fig. 10b plots the phase-trajectory with data taken from $t = 500 - 700$, and it suggests the second-well is due to the

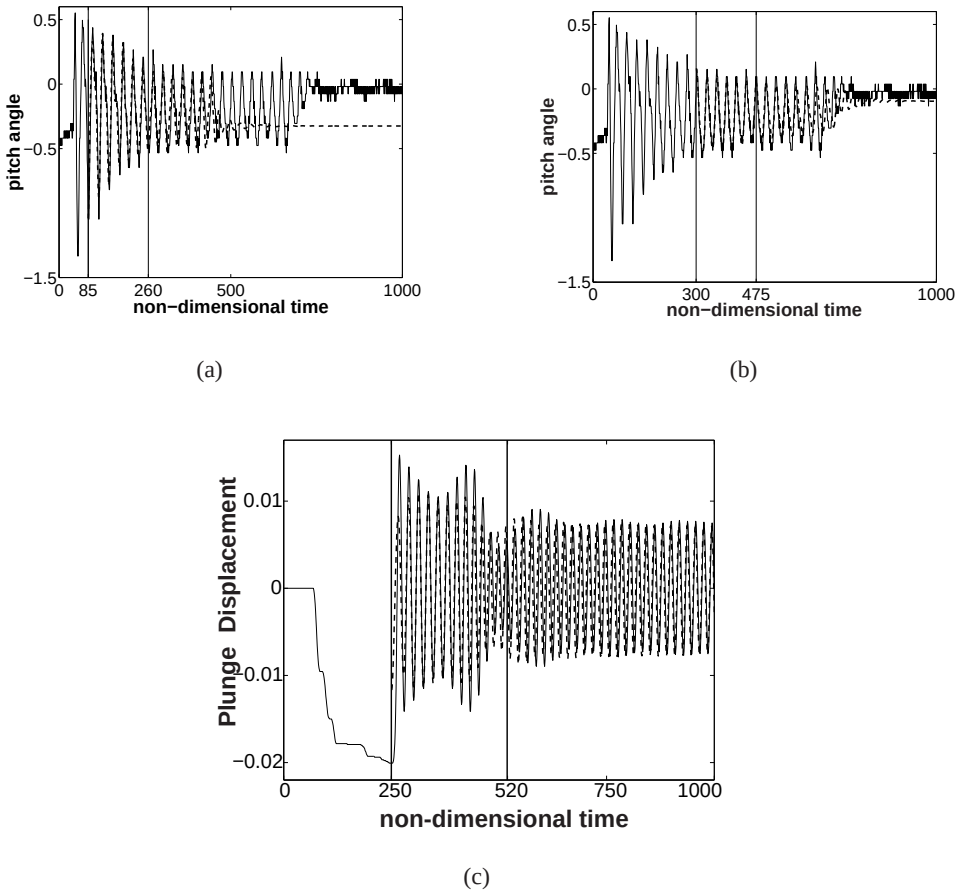

Figure 8: Experimental and predicted aeroelastic response (a)- (b) freeplay (c) polynomial spring

segment of the time series from $t = 600 - 700$. In Fig. 10c, we display the phase space for the last 500 data taken from $t = 500 - 1000$, and we can clearly see the two-well potential is well developed.

It should be noted that although the predicted time history may not overlap with the original data, but the characteristics of a chaotic motion can still be extracted from the reconstructed phase-trajectory. We now compare the phase plots from the numerical simulated data and those resulting from the prediction. Fig. 11a shows the predicted phase-space from $t = 0 - 1000$ using the first 200 data in Fig. 9 as input for the nonparametric study and parameter estimations. The plot is somewhat different with that shown in Fig. 10d, in particular, it shows a one-well potential behavior rather that a two-well potential. However, Fig. 11a is in a good agreement with the phase plot using the first 600 data from the original time series shown in Fig 10a. As we have mentioned earlier that the pitch motion

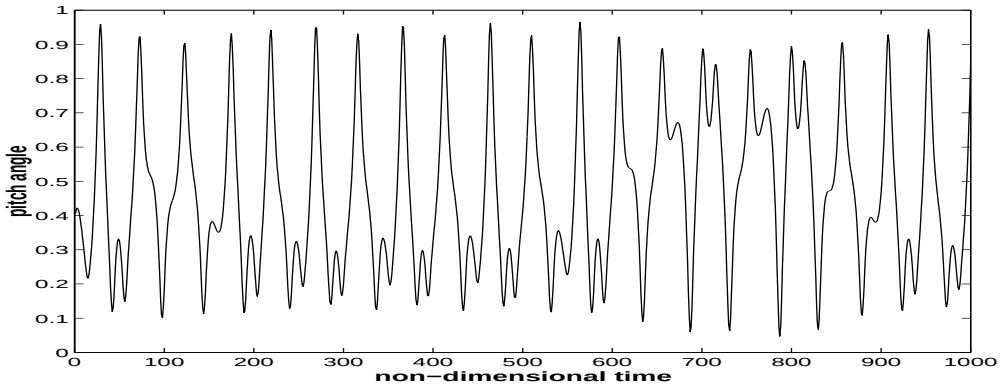

Figure 9: Simulated chaotic data

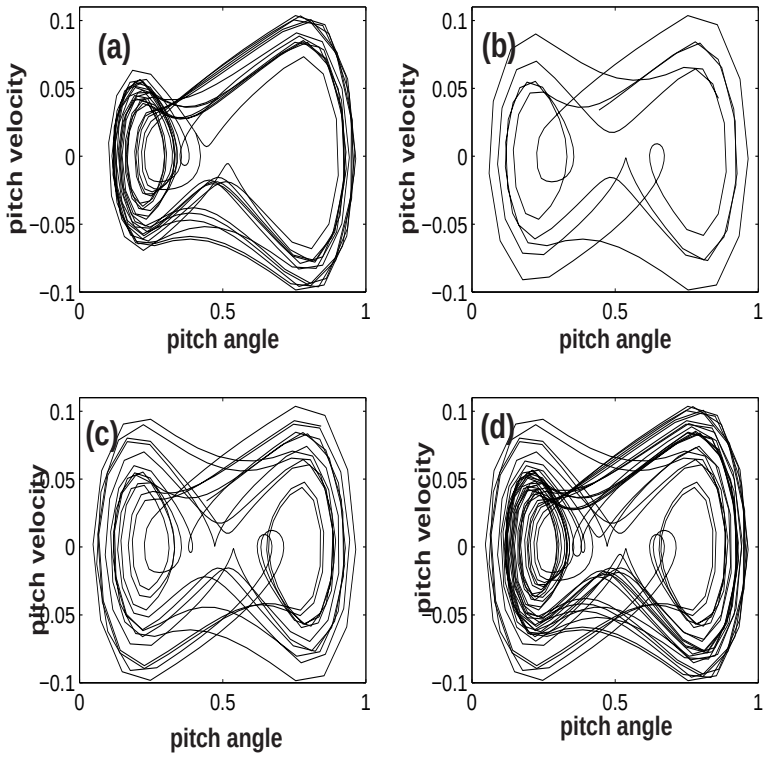

Figure 10: Phase space for the chaotic data with t (a) 0-600 (b) 500-700 (c) 500-1000 (d) 0-1000

exhibits a significant change during the time 600-700, and this is likely the cause in contributing the second well potential. Fig. 10c illustrates the phase plot of the chaotic motion using the data from 500-1000. Using 200 data taken from 500-700

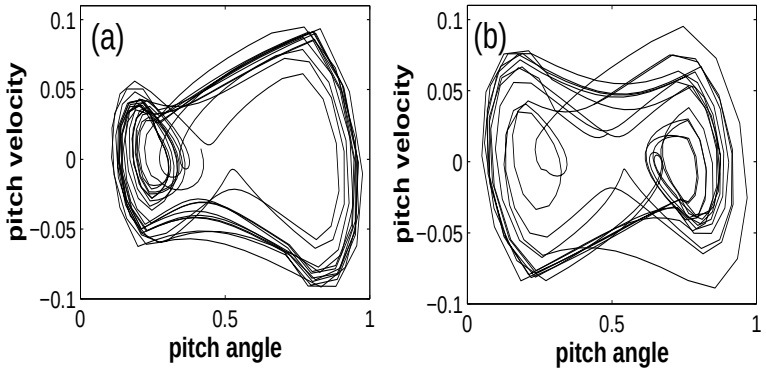

Figure 11: Predicted phase space with input data taken from (a) 0-200 (b) 500-700

of the original time series as input, the predicted phase plot using 500 data shown in Fig. 11b is in a reasonable agreement with that displayed in Fig. 10c. Even though the preliminary results are encouraging, more detail investigations are needed for cases with chaotic motions.

6 CONCLUSIONS

A data-driven method is developed to predict the steady state response for nonlinear aeroelastic systems. Utilizing the known transient data as input, the method first identifies the specific type of nonlinearity using nonparametric statistical method. Appropriate state-space models are then proposed to model aeroelastic systems with continuous or piece-wise linear structural nonlinearity. The system parameters are estimated by applying the Kalman filter and the expectation maximization algorithm. Consequently, the nonlinear aeroelastic behavior is forecasted from the reconstructed state-space models.

The approach has been tested on transient data generated from experiments and numerical simulations. It has been demonstrated the nonparametric method is capable of identifying the presence of the switching points. Hence, nonlinearity associated with freeplay and hysteresis can be distinguished from a polynomial spring. From the information of the structural nonlinearity, we proposed a switching linear state-space model or a nonlinear model for an aeroelastic system with piece-wise linear or continuous structural nonlinearity. The proposed method has been tested in which the nonlinear behaviors correspond to limit-cycle-oscillation, fixed-point solution, divergent and chaotic motion.

The aeroelastic model discussed in this paper contains a nonlinearity arising only from the structures. In future study, it will be of interest to test the method when the aeroelastic data are resulted from system with both the aerodynamic non-

linearity and the structural nonlinearity.

ACNOLEWDGEMENTS

The authors would like to thank Dr. C. Marsden of McGill University, Dr. T. Strganac of Texas A&M University, and Dr. L. Liu of North Carolina Agricultural & Technical State University for providing the aeroelastic response data sets in our study. The authors would also like to acknowledge the support received from the Natural Sciences and Engineering Research Council of Canada.

References

[1] A. Balakrishnan. *Kalman Filtering Theory*. Optimization Software, Inc., New York, 1984.

[2] D. Brillinger and M Rosenblatt. Asymptotic theory of kth order spectra. In B. Harris, editor, *Spectral analysis of time series*, pages 153–158. John Wiley, New York, 1989.

[3] C. C. Chabalko, M. R. Hajj, D. T. Mook, and W. A. Silva. Characterization of the LCO response behaviors of the NATA model. In *Proceedings of the 47th AIAA/ ASME/ ASCE/ AHS/ ASC/ Structures, Structural Dynamics, and Materials Conference*, Newport, RI, USA, 2006. AIAA Paper 2006-1852.

[4] M. D. Conner, D. M. Tang, E. H. Dowell, and L.N. Virgin. Nonlinear behavior of a typical airfoil section with control surface freeplay. *Journal of Fluids and Structures*, 11:89–109, 1997.

[5] E.H. Dowell, J. W. Edwards, and T. Strganac. Nonlinear aeroelasticity. *Journal of aircraft*, 40:857–874, 2003.

[6] M.R. Hajj and W. A. Silva. Nonlinear flutter aspects of the flexible high-speed civil transport semispan model. *Journal of aircraft*, 41:1202–1208, 2004.

[7] N. Jacsic, M. Boltezar, I. Simonovski, and A. Kuhelj. Dynamical behaviour of the planar non-linear mechanical system - Part i: Theoretical modeling. *Journal of Sound and Vibration*, 5(226):923–940, 1999.

[8] S. Julier, J.K. Uhlmann, and H.F. Durrant-White. A new method for the nonlinear transformation of means and covariances in filters and estimators. *IEEE Trans. Aut. Control*, 45(3):477–482, 2000.

[9] Y. Kim and E. Powers. Digital bispectral analysis of self-excited fluctuation spectra. *The Physics of fluids*, 21:1452–1453, 1978.

[10] B. H. K. Lee, S. J. Price, and Y. S. Wong. Nonlinear aeroelastic analysis of airfoils: bifurcation and chaos. *Progress in Aerospace Sciences*, 35:205–334, 1999.

[11] K. Lii, M. Rosenblatt, and C. Van Atta. Bispectral measurements in turbulence. *Journal of fluid mechanics*, 77:45–62, 1976.

[12] L. Liu, Y.S Wong, and B.H.K. Lee. Application of the centre manifold theory in nonlinear aeroelasticity. *Journal of Sound and Vibration*, 234:641–659, 2000.

[13] X.L. Meng and D. Van Dyk. The EM algorithm - an old folk-song to a fast new tune. *J.R. Statist. Soc.B*, 59(3):511–567, 1997.

[14] R.M. Neal and G.E. Hinton. A view of the EM algorithm that justifies incremental, sparse, an other variants. In M.I. Jordan, editor, *Learning in Graphical Models*. 1998.

[15] C. Popescu, Y.S. Wong, and B.H.K. Lee. An expert system for predicting non-linear aeroelastic behavior of an airfoil. *Journal of Sound and Vibration*, 2008 (submitted).

[16] C. A. Popescu and Y. S. Wong. A nonlinear statistical approach for aeroelastic response prediction. *AIAA J. Guid.,Contr., Dynamics*, 26(4):565–572, 2003.

[17] C. A. Popescu, Y. S. Wong, and B. H. K. Lee. System identification for nonlinear aeroelastic models. In *Proceedings of the 46th AIAA/ ASME/ ASCE/ AHS/ ASC/ Structures, Structural Dynamics, and Materials Conference*, Austin, TX, USA, 2005. AIAA Paper 2005-1855.

[18] S.J. Price, H. Alighambari, and B.H.K. Lee. The aeroelastic response of a two-dimensional airfoil with bilinear and cubic structural nonlinearities. *Journal of Fluids and Structures*, 9:175–193, 1995.

[19] R.H. Shumway and D.S. Stoffer. An approach to time series smoothing and forecasting using the EM algorithm. *J. Time Ser. Anal.*, 3(4):253–264, 1982.

[20] W. A. Silva and S. Dunn. Higher order spectral analysis of F-18 flight flutter data. In *Proceedings of the 46th AIAA/ ASME/ ASCE/ AHS/ ASC/ Structures, Structural Dynamics, and Materials Conference*, Austin, TX, USA, 2005. AIAA Paper 2005-2014.

[21] W. A. Silva, T. W. Strganac, and M. R. Hajj. Higher-order spectral analysis of a nonlinear pitch and plunge apparatus. In *Proceedings of the 46th AIAA/ ASME/ ASCE/ AHS/ ASC/ Structures, Structural Dynamics, and Materials Conference*, Austin, TX, USA, 2005. AIAA Paper 2005-2013.

[22] H. Tong. *Nonlinear Time Series*. The Clarendon Press Oxford University Press, New York, 1990.

[23] C. Van Atta. Inertial range bispectra in turbulence. *The Physics of fluids*, 22:1440–1442, 1979.

[24] O. Voitcu and Y. S. Wong. Neural network approach for nonlinear aeroelastic analysis. *AIAA J. Guid.,Contr., Dynamics*, 26(1):99–105, 2003.

[25] Y.S. Wong, O. Voitcu, and C.A. Popescu. An expert data mining system for nonlinear aeroelastic response prediction. In *Proceedings of the International Council of the Aeronautical Sciences Congress*, Toronto, ON, Canada, 2002.

[26] C.F.J. Wu. On the convergence properties of the EM algorithm. *The Annals of Statistics*, 11(1):95–103, 1983.